# NMR Imaging of the Spine

Jong S. Han, Benjamin Kaufman, Saba J. El Yousef, Jane E. Benson, Charles T. Bonstelle, Ralph J. Alfidi, John R. Haaga, Hong Yeung and Richard G. Huss

*AJNR Am J Neuroradiol* 1983, 4 (6) 1151-1159
http://www.ajnr.org/content/4/6/1151

# NMR Imaging of the Spine

Jong S. Han[1]
Benjamin Kaufman[1]
Saba J. El Yousef[1]
Jane E. Benson[1]
Charles T. Bonstelle[1]
Ralph J. Alfidi[1]
John R. Haaga[1]
Hong Yeung[2]
Richard G. Huss[1]

**The usefulness of nuclear magnetic resonance (NMR) images in the evaluation of spinal disorders below the craniocervical junction was studied. Six normal subjects and 41 patients with various spinal abnormalities were examined. NMR proved capable of demonstrating important normal and pathologic anatomic structures; it was useful in the evaluation of syringohydromyelia and cystic spinal cord tumors, and the bright signal intensity of lipoma was quite impressive. In the evaluation of herniated disk, NMR images offered a new perspective by visualizing abnormal degradation of the signal intensity of the nucleus pulposus itself. NMR images were least valuable in the evaluation of spondylosis and spinal stenosis. Although NMR imaging of the spine is still in a very early developmental stage, the absence of both ionizing radiation and risks associated with contrast material makes it especially attractive as a new diagnostic method. This limited experience with currently available equipment suggests that, with technical refinement, the efficacy of NMR of the spine will increase.**

Nuclear magnetic resonance (NMR) holds great promise as an imaging method, with its high theoretical limits in image detail and very low attendant risks. Clinical experience in the evaluation of the central nervous system, particularly the brain, is rapidly accumulating [1–5]. However, the normal anatomic features of the spine have not been established thus far with NMR. We summarize initial NMR studies of spinal anatomy in normal subjects at our institution and present NMR findings in a spectrum of spinal pathology.

## Subjects and Methods

During a 5-month period, six normal subjects and 41 patients with various spinal abnormalities underwent NMR examinations at Case Western Reserve University/University Hospitals of Cleveland. Normal adult volunteers included four men and two women with a mean age of 31 years. To delineate the normal morphologic images of the spine and its related structures, the entire spinal column of each normal subject was studied in a supine position. NMR studes were also performed on 41 patients (20 men and 21 women; age range, 12–77 years; mean age, 37 years) who had a confirmed diagnosis on the basis of clinical findings and/or preceding radiologic studies, including myelography and computed tomography (CT). Written informed consent was obtained from all participants.

Various radiofrequency pulse sequences were used to obtain the NMR images, including saturation-recovery (SR), inversion-recovery (IR), and $T_2$-weighted spin-echo (SE) pulse sequences. The principles describing these sequences and the technique of NMR imaging have been described [4–8]. The NMR imaging system that we currently use is a Cryogenic Superconducting Magnet (Teslacon, Technicare Corp., Solon, OH) with a 100 cm bore, operating at 3.0 kG. The NMR scan was generated using a two-dimensional Fourier transform technique with 128 phase-encoding data lines. The data acquisition time varies depending on the pulse sequences used. The SR technique (0.5 sec sequence interval, 30 msec echo delay) requires 2.3 min; the IR technique (1.5 sec sequence interval, 30 msec echo delay and 450 msec inversion time), 6.7 min; and the $T_2$-weighted SE technique (1.0 sec sequence interval, 60 msec echo delay), 4.5 min. The slice thickness is about 10 mm.

**This article appears in the November/December 1983 issue of *AJNR* and the December 1983 issue of *AJR*.**

Received May 5, 1983; accepted after revision July 19, 1983.

Presented at the annual meeting of the American Society of Neuroradiology, San Francisco, June 1983.

[1]Department of Radiology, Case Western Reserve University School of Medicine, University Hospitals of Cleveland, 2074 Abington Rd., Cleveland, OH 44106. Address reprint requests to J. S. Han.

[2] Technicare Corporation, Solon, OH 44139.

**AJNR 4:1151–1159, Nov/Dec 1983**
0195-6108/83/0406-1151 $00.00

TABLE 1: **Gray Scale of NMR Images in the Spine and Related Structures**

| Gray Scale from Brightest to Darkest |
|---|
| Brightest (high proton density; short $T_1$ and/or long $T_2$) |
| Fat |
| Nucleus pulposus ($T_2$-weighted SE technique) |
| Marrow cavity and cancellous bone |
| Nucleus pulposus (SR technique) |
| Spinal cord |
| Muscle |
| CSF |
| Anulus fibrosus |
| Ligaments |
| Compact, cortical bone |
| Darkest (very low proton density; long $T_1$ and/or short $T_2$) |

These studies were done using a body coil with an aperture size of 55 cm. The upper cervical spine (C1–C4) was also studied using a head coil with an aperture of 29 cm.

## Results

### *Normal Spine*

Sagittal, coronal, and axial NMR images were obtained to evaluate the normal spine. The relative intensities of the spine and related anatomic structures on the NMR images are listed in table 1. In the evaluation of the normal and abnormal spine, SR NMR images were found to provide the best spatial resolution and anatomic detail. In both IR and $T_2$-weighted SE images, the spatial resolution was relatively

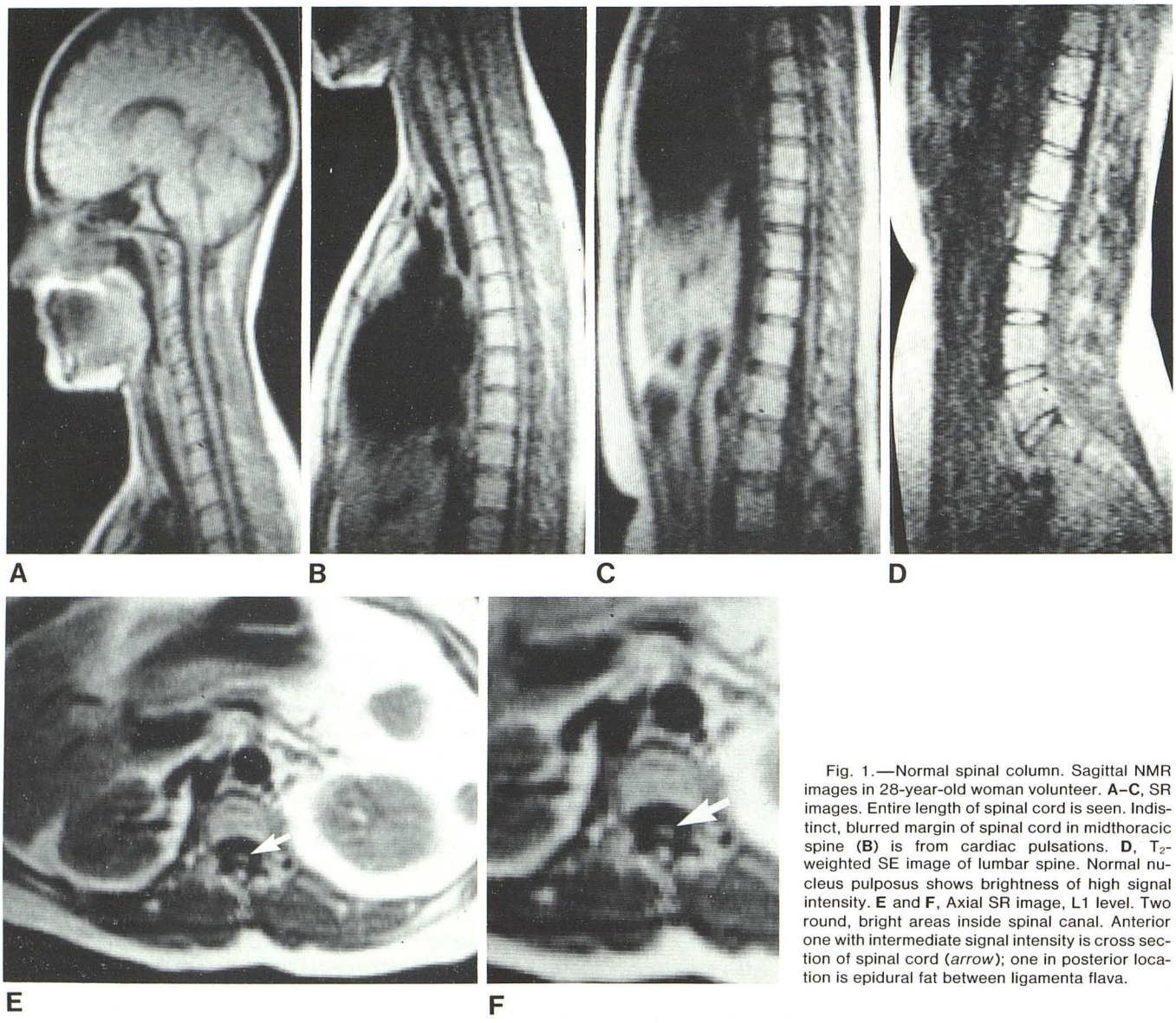


Fig. 1.—Normal spinal column. Sagittal NMR images in 28-year-old woman volunteer. **A–C**, SR images. Entire length of spinal cord is seen. Indistinct, blurred margin of spinal cord in midthoracic spine (**B**) is from cardiac pulsations. **D**, $T_2$-weighted SE image of lumbar spine. Normal nucleus pulposus shows brightness of high signal intensity. **E** and **F**, Axial SR image, L1 level. Two round, bright areas inside spinal canal. Anterior one with intermediate signal intensity is cross section of spinal cord (*arrow*); one in posterior location is epidural fat between ligamenta flava.

TABLE 2: **Initial Clinical Experience with NMR of the Spine**

| Location: Pathology | No. of Cases |
|---|---|
| Intramedullary: | |
| Syringohydromyelia | 5 |
| Spinal cord tumor | 3 |
| Demyelination of spinal cord | 2 |
| Intradural extramedullary: | |
| Neurofibroma | 3 |
| Meningioma | 1 |
| Extradural: | |
| Arachnoid cysts (diverticula) | 3 |
| Metastases | 5 |
| Eosinophilic granuloma | 1 |
| Compression fracture | 1 |
| Herniated disk | 5 |
| Bulging disk | 1 |
| Spondylosis | 3 |
| Spinal stenosis | 1 |
| Ankylosing spondylitis | 1 |
| Combined: | |
| Neurofibromatosis | 3 |
| Lipoma | 1 |
| Spinal dysraphism | 2 |
| Total | 41 |

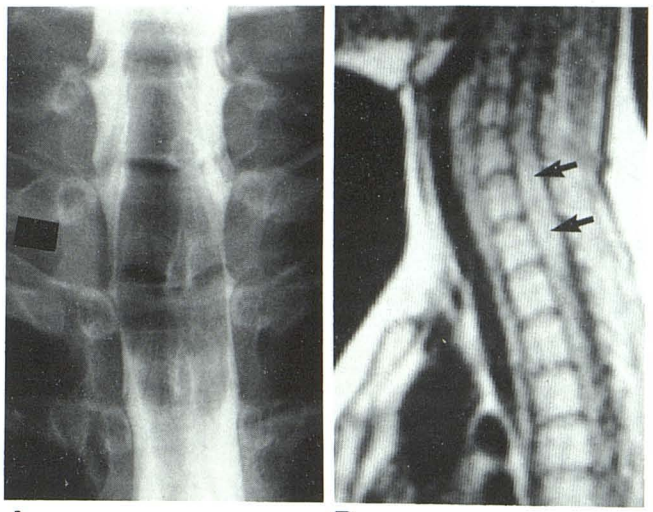

A B

Fig. 4.—Cystic astrocytoma. **A**, Metrizamide myelogram. Fusiform enlargement of spinal cord at T1–T2 level. **B**, SR image reveals not only fattened cord but also low signal intensity of central, cystic component of intramedullary tumor (*arrows*).

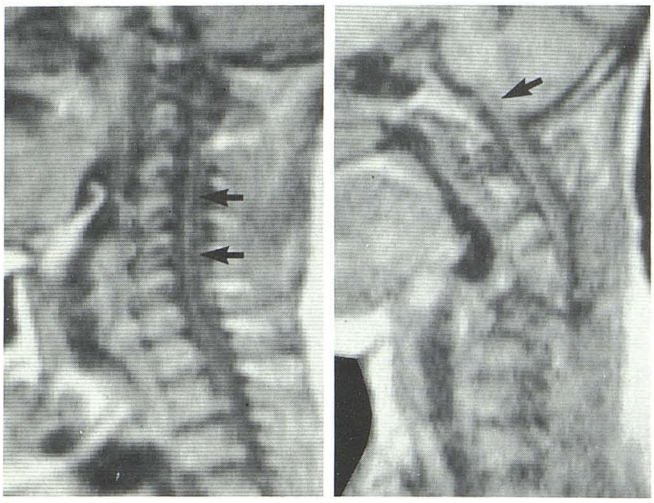

2 3

Fig. 2.—SR image of 61-year-old man with syringohydromyelia. Low signal intensity of cystic cavity is seen through central part of cervical spinal cord (*arrows*).

Fig. 3.—SR image of 38-year-old man who has "swan-neck" deformity from previous compression fractures of C4, C5, and C6 vertebrae. Syringohydromyelia extending into medulla is seen clearly (*arrow*). Metrizamide myelography followed by CT showed enlargement of cervical spinal cord but failed to show collection of metrizamide in syrinx cavity.

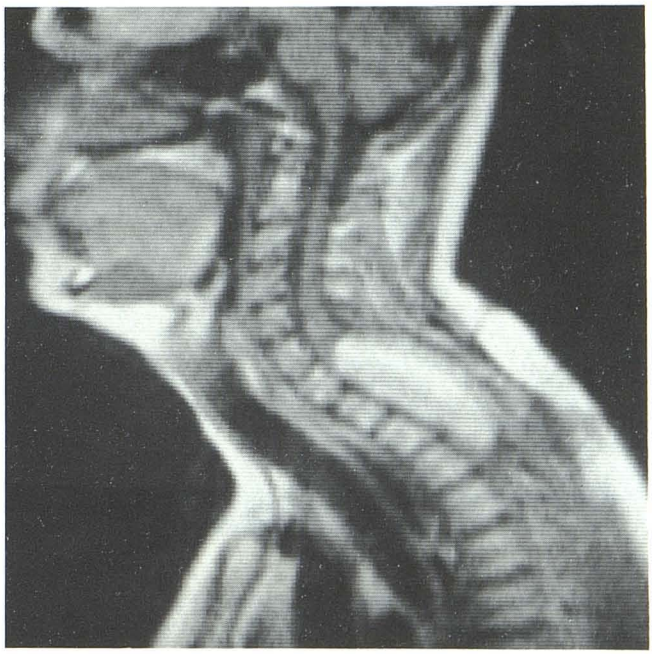

Fig. 5.—SR image of lipoma. Bright signal intensity of tumor delineates its entire extent in thoracic spine. Heterogeneous intensity in ventral part of lipoma is probably related to mixture of signals from intramedullary lipoma and spinal cord.

poor and no additional information was obtained except accentuated brightness of nucleus pulposus in $T_2$-weighted SE image.

Using the body coil and sagittal SR images, the vertebral bodies, intervertebral disks, and intraspinal canal contents were well visualized (figs. 1A–1D). The cancellous bone-containing marrow cavity within the vertebral bodies exhibited high signal intensity, and appeared bright surrounded by very low signal intensity from the compact cortical bone. Two transverse lines of intermediate signal intensity were noted within the vertebral bodies in young individuals. These probably represent endochondral ossification centers. The anterior and posterior longitudinal ligaments appeared as areas of low signal intensity and could not be separated from the adjoining cortical bone of vertebral bodies. The nucleus pulposus exhibited a high signal intensity in contrast to the low intensity of the surrounding

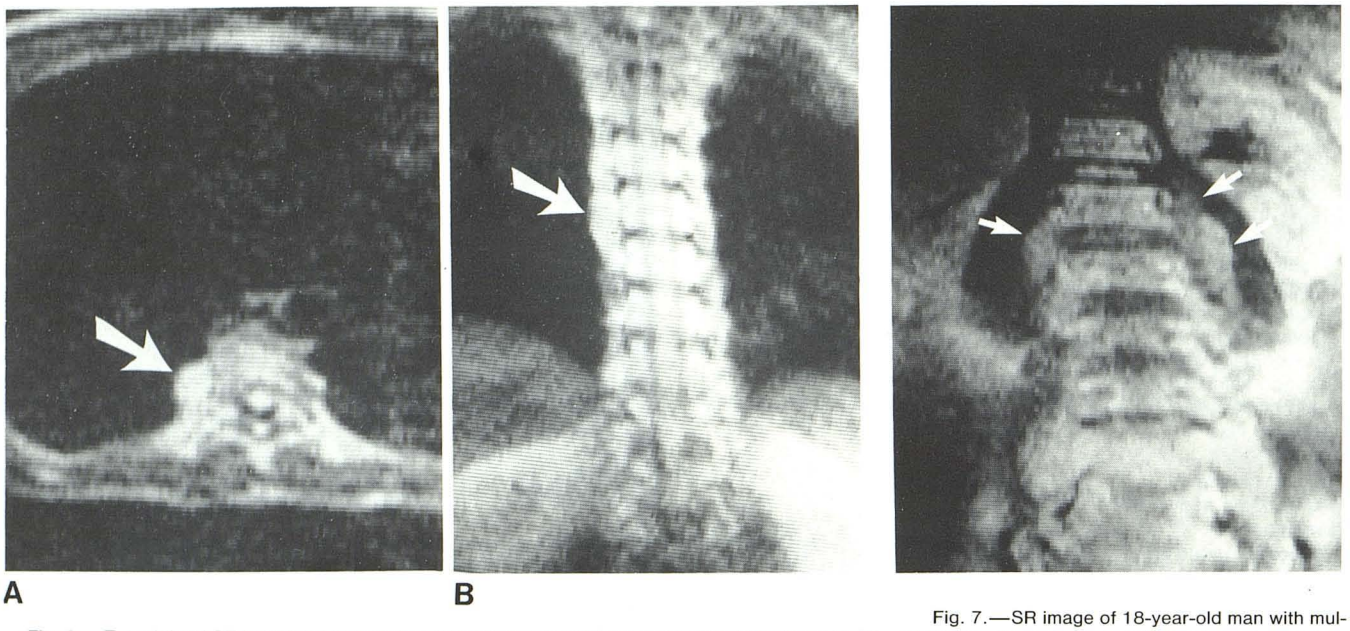


Fig. 6.—$T_2$-weighted SE images of extradural neurofibroma in axial (**A**) and coronal (**B**) planes at T7 level (*arrows*). Coronal plane also reveals thoracic spinal cord surrounded by low signal intensity of CSF.

Fig. 7.—SR image of 18-year-old man with multiple neurofibromas. Coronal plane in lumbar region. Extradural neurofibromas extend down along medial aspect of psoas muscle bilaterally (*arrows*).

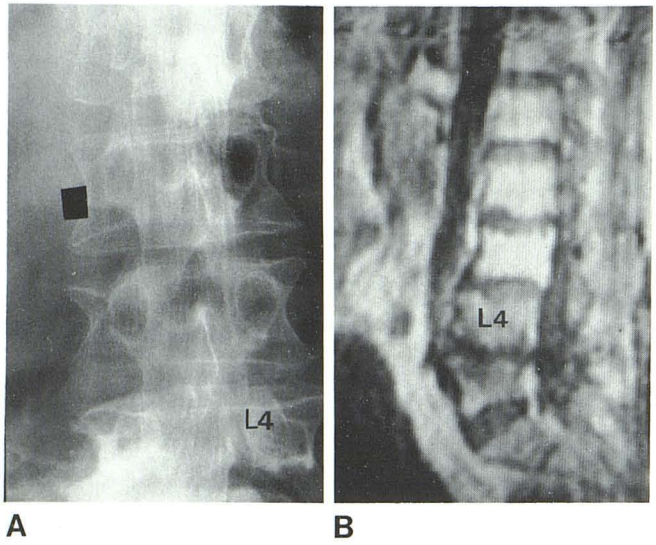


Fig. 8.—Multiple neurofibromas. **A**, Myelogram. Limited filling of metrizamide below L2 level because of multiple intradural tumors. **B**, SR image clearly reveals abnormal intermediate signal intensity of tumor masses in thecal sac, particularly well seen at L4 level. NMR showed significant degenerative intervertebral disk disease with bony changes along vertebral endplates at L4–L5 level.

anulus fibrosus. The difference in the width of the anulus fibrosus between the anterior and posterior compartments of a disk was clearly shown in sagittal images. In $T_2$-weighted SE images, the signal intensity of the nucleus pulposus was markedly exaggerated compared with the surrounding structures. This appears to be a significant finding in the evaluation of the abnormal disk, as will be discussed later. The spinal cord was clearly visualized as a structure exhibiting intermediate signal intensity surrounded by an area of low signal intensity emanating from cerebrospinal fluid (CSF), thecal sac, and a composite of epidural structures, including the posterior longitudinal ligament and vertebral body cortex.

In the lumbar region, the conus medullaris was seen adequately. The nerve roots and the filum terminale could not be seen as structures separate from the surrounding CSF.

In parasagittal images, the pedicles and intervertebral neural foramina were seen. Axial images provided better morphologic delineation of the posterior elements of the spine, almost equivalent to late-generation CT images without the magnification mode (figs. 1E and 1F). The high signal intensity of extradural fat between the ligamentum flavum and posterior to the thecal sac was almost always seen in the lower thoracic and lumbar regions.

Due to the normal curvature of the spine, it was time-consuming to obtain coronal images, particularly when a large area of the spine was to be examined. There was significant degradation on both sagittal and coronal NMR images in patients with sclerosis and in those who were not positioned parallel to the long axis of the Z coil on the NMR scanner.

In several subjects, images of the upper cervical spine were obtained with a head coil. These NMR images were superior to those obtained with a body coil.

### *Abnormal Spine*

The pathologic entities and number of patients studied are summarized in table 2.

*Syringohydromyelia.* In four of five patients with clinically diagnosed syringohydromyelia, sagittal NMR images clearly

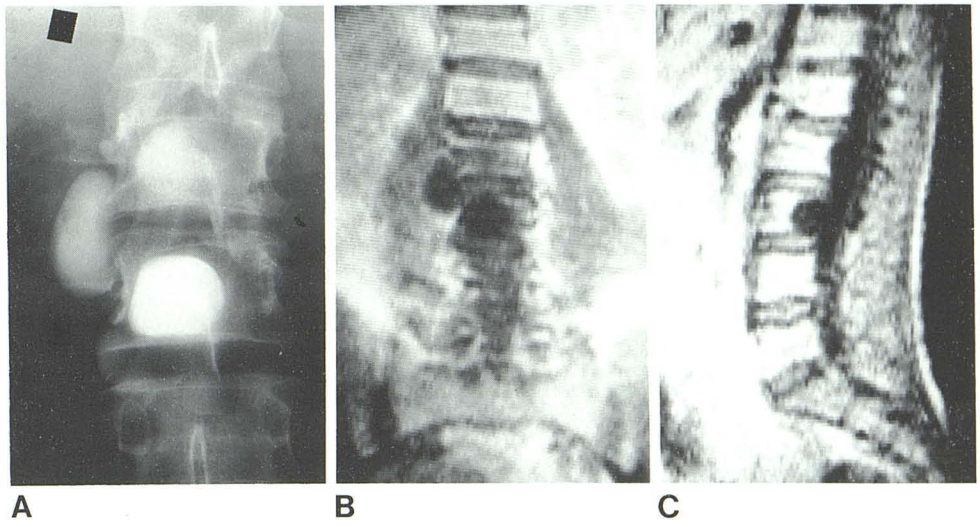


Fig. 9.—Multiple meningoceles in patient with neurofibromatosis. **A**, Anteroposterior view of lumbar spine from metrizamide myelography in prone position. Coronal (**B**) and sagittal (**C**) SR images. Low signal intensity of meningoceles is seen sharply relative to adjacent psoas muscle and vertebrae.

showed the low signal intensity of the tubular CSF-containing central cavity within the spinal cord (fig. 2). Extension of the syrinx into the medulla was well demonstrated in one patient (fig. 3). In the fifth case where no abnormality was seen on NMR images, no evidence of syringohydromyelia could be found at surgery.

*Spinal cord tumors.* NMR clearly depicted enlargement of the spinal cord and the extent of the tumor in two patients with intramedullary tumors of the thoracic region. There was no apparent change in signal intensity between the tumor and normal spinal cord. In one patient with intramedullary astrocytoma, a linear, low signal intensity was observed at the center of the enlarged cord (fig. 4). At surgery, this was shown to represent a cystic component of the spinal cord tumor.

In a case of ependymoma of the conus medullaris, with complete block from below on metrizamide myelography, NMR was able to delineate the upper extent of the tumor, obviating additional study by lateral C1–C2 puncture approach. The very bright signal intensity peculiar to fat was seen in a patient with intramedullary lipoma with exophytic components into the intradural subarachnoid space (fig. 5).

*Demyelinating disorders.* Unlike NMR images of the brain, the gray and white matter of the spinal cord could not be differentiated using our current techniques. In two patients with clinically suspected demyelinating disorders of the thoracic spinal cord, no definite abnormalities were seen.

*Neurofibromatosis.* Six cases were studied demonstrating multiple neurofibromas and dural ectasia. In a patient with extradural neurofibroma in the thoracic region, the paraspinal extension of the tumor from the neural exit was visualized well (fig. 6). In another patient, extradural neurofibromas, this time involving the lumbar area, were seen clearly contrasted against adjacent psoas muscles (fig. 7). In yet another patient with multiple neurofibromas in the lumbar intradural space, NMR showed abnormal intermediate signal intensity of the tumors in the thecal sac (fig. 8). The low-signal-intensity, CSF-filled meningoceles in a case of dural ectasia were clearly delineated from adjacent structures (fig. 9). In two cases with intradural extramedullary neurofibromas less than 5 mm in size, the lesions were not identified in NMR images.

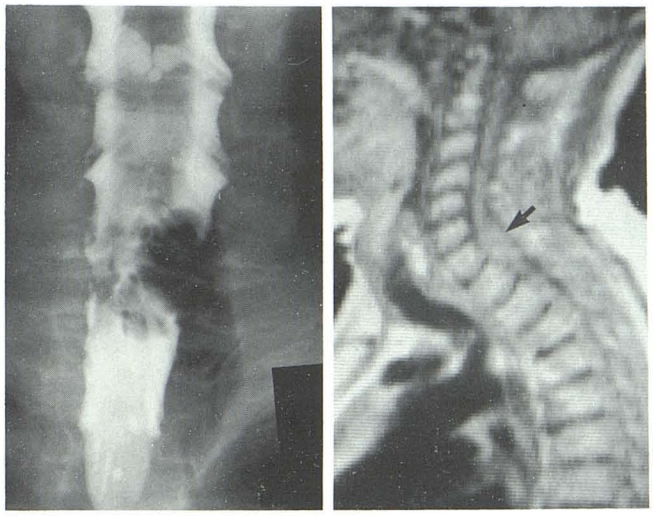


Fig. 10.—Meningioma. **A**, Pantopaque myelogram. Intradural extramedullary mass at C7–T1 level on left side. **B**, SR image in sagittal plane. Apparent widening of spinal cord is seen at same level (*arrow*). Coronal images were not obtainable because of patient's poor condition.

*Meningioma.* One case was studied of intradural extramedullary meningioma of the C7–T1 region. The accentuated kyphosis of the thoracic spine prevented adequate positioning. On the few slices obtained in the sagittal position, the spinal cord appeared widened in its anteroposterior dimension, simulating an intramedullary lesion (fig. 10). However, we believe that sections through the meningioma itself were not obtained, and the apparent widening very well could have been the result of flattening of the cord by extrinsic compression from the laterally situated meningioma.

*Extradural arachnoid cysts (diverticula).* Extradural cysts

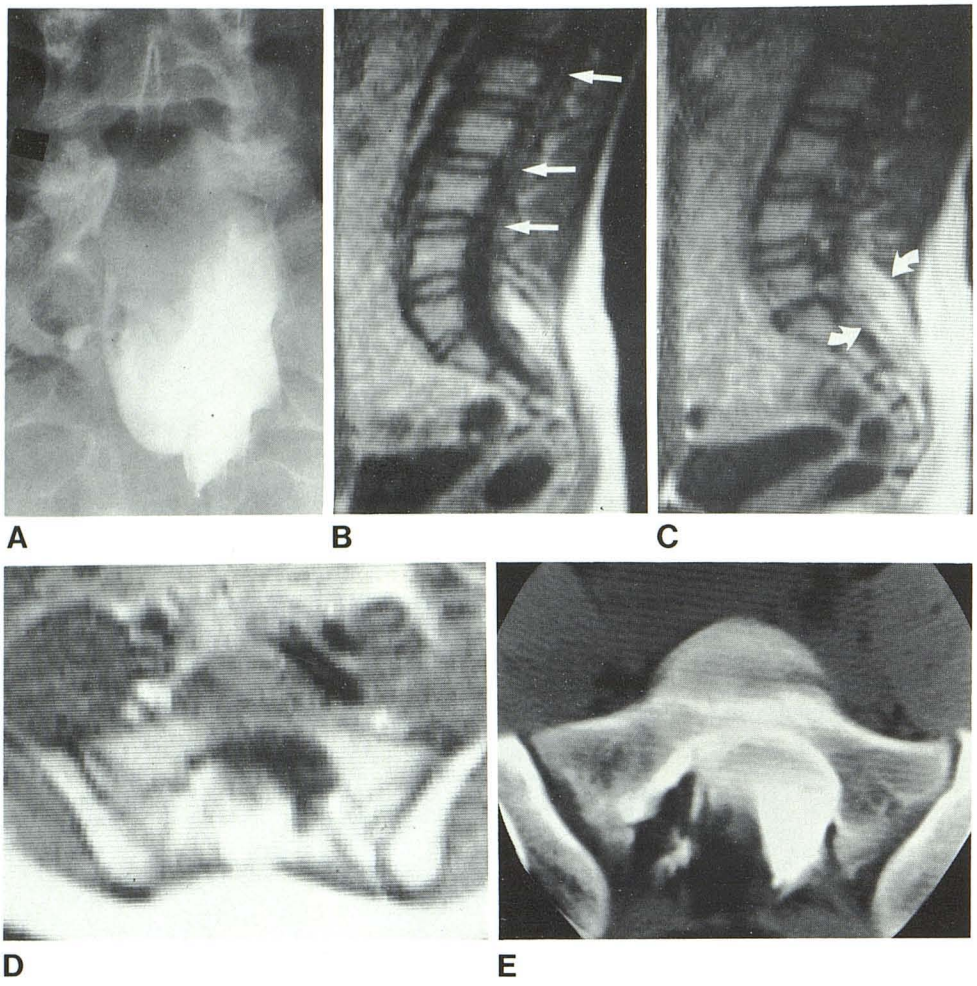


Fig. 11.—Spinal dysraphism in 15-year-old boy. **A**, Metrizamide myelogram. Separation of low-lying spinal cord from lipoma is impossible on myelogram. Superior extent of lipoma was not apparent because of rapid dilution of metrizamide in capacious subarachnoid space. **B**, Sagittal SR image shows low-lying spinal cord along posterior aspect of capacious thecal sac (*arrows*). **C**, Parasagittal image toward right side shows larger part of lipoma (*arrows*). Pedicles and intervertebral foramina at L3 level through S1 are seen clearly in this image plane. **D**, Axial NMR image at S1 level shows composition of intra- and extradural lipoma. **E**, CT scan after myelography shows nearly identical configuration of intra- and extradural lipoma, as in NMR images. With NMR, white intensity represents fat and black is CSF; with CT, white density is CSF mixed with metrizamide, and black is fat.

in the thoracic region were studied in three cases. In two, there was apparent widening of the posterior aspect of the subarachnoid space. However, the cyst could not be seen separate from adjoining extradural structures.

*Spinal dysraphism.* Two patients were studied with spinal dysraphism associated with tethered cord. In both cases, NMR images demonstrated dural ectasia and a low-lying spinal cord. In one case, the cohesion of an intra- and extradural lipoma was seen clearly (fig. 11).

*Bony (vertebral body) abnormalities.* Five patients with metastases were studied, one with eosinophilic granuloma and one with minimal compression fracture of the vertebral body. In metastatic disease, the bony destruction and marrow replacement by tumor significantly altered the signal intensity of the marrow from bright to intermediate (fig. 12A). Soft-tissue extension of the tumor was also seen (figs. 12B and 12C). Figure 13 illustrates one case where vertebral body collapse due to metastasis was better visualized on the NMR image than on the corresponding radiograph. In one patient with eosinophilic granuloma of the thoracic spine, the destruction of the vertebral body and associated paraspinal mass was seen well (fig. 14). The appearance on NMR could not be distinguished from a metastatic lesion. NMR images did not show any abnormality in the patient with a minimally compressed acute fracture of the T4 vertebral body.

*Spinal stenosis/spondylosis.* Three patients with spondylosis of the cervical spine and one patient with lumbar spinal stenosis were studied. Spondylosis, as seen on myelography, was not demonstrable with NMR. In one patient, degenerative spurs at the C5–C6 level associated with indentation of the spinal cord were clearly identified in sagittal NMR images (fig. 15); however, smaller abnormalities at the C4–C5 and C6–C7 levels seen in the corresponding myelogram could not be appreciated. NMR also failed to show abnormalities in a patient with a moderate degree of central stenosis of the lumbar spine and in one case of ankylosing spondylitis.

*Lumbar disk herniation.* Five cases of herniated disk at the L4–L5 and/or L5–S1 levels were studied. The herniated disks, subsequently proven at surgery, were the only abnormality involving the spine diagnosed in these patients. With NMR, herniation of the disks could not be seen. However, in all cases, the signal intensity of the nucleus pulposus at the abnormal, herniated disk level was significantly reduced (fig. 16). A similar finding of decreased signal inten-

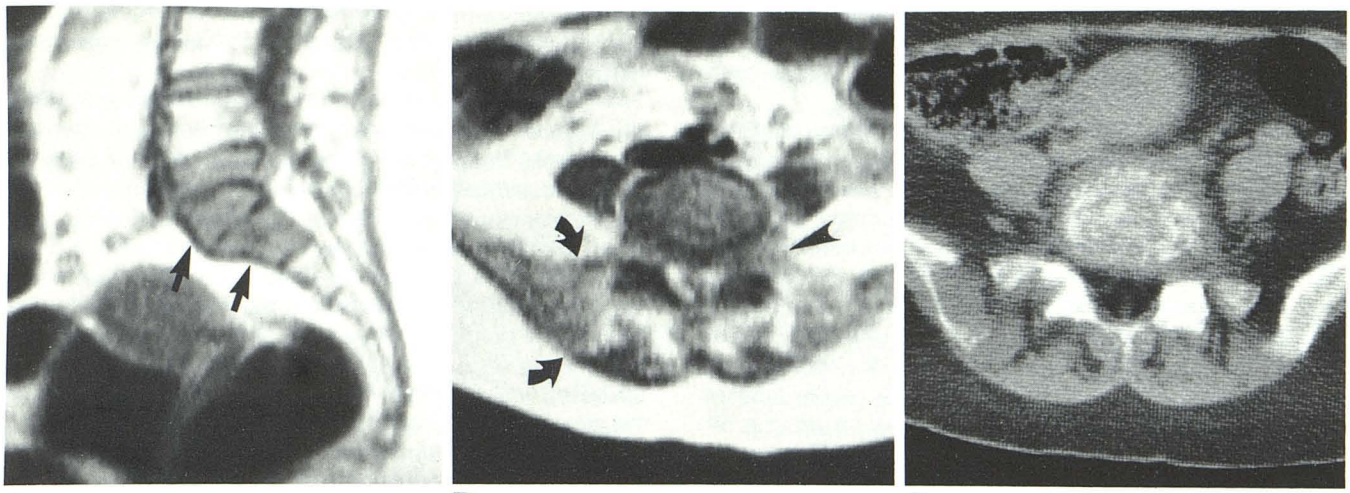

A B C

Fig. 12.—Metastasis from bronchogenic carcinoma. **A**, SR image. Abnormal, low signal intensities of marrow cavities of S1 and S2 (*arrows*). Plain radiographs on same day did not reveal abnormality in area. **B**, Axial NMR image at L5–S1 level. Large area of abnormal signal intensity in ilium at superior end of sacroiliac joint on right side (*arrows*) extending posteriorly. Abnormal signal intensity also in region of intervertebral foramen on left side (*arrowhead*). These findings are quite compatible with axial CT scan (**C**) at the same level.

Fig. 13.—Metastasis from breast carcinoma. **A**, Lateral view during myelogram. Extradural defect at L5 level and slightly collapsed L5 vertebral body. **B**, Sagittal SR image clearly depicts abnormal signal intensity of collapsed L5 vertebral body protruding into spinal canal (*arrow*).

Fig. 14.—Eosinophilic granuloma in 12-year-old boy. Sagittal SR image shows abnormal, heterogeneous signal intensity of vertebral body at T11. Adjacent soft-tissue mass with high signal intensity represents paraspinal extension of abnormality (*arrow*).

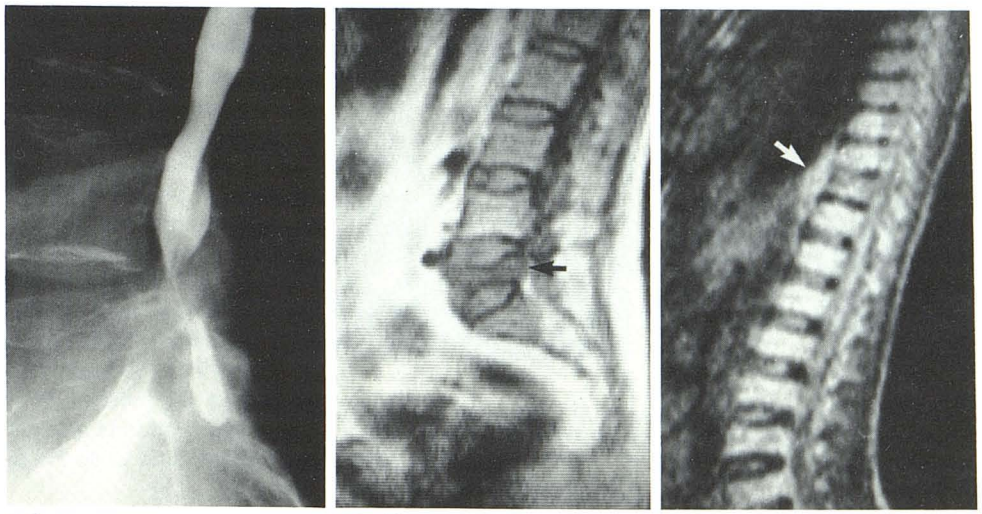

13 A 13 B 14

sity of nucleus pulposus was also observed in a patient who had minimal protrusion of the disks without apparent herniation (fig. 17).

## Discussion

NMR imaging of the spine shows considerable diagnostic potential even in its current state of development. It is preferable to CT and myelography because it uses no ionizing radiation or contrast agents, and direct multiplanar images are obtainable. Our initial experiences show NMR has much to offer, both as an adjunct to current techniques and as a primary diagnostic method in its own right. However, long imaging time, in the range of minutes with current NMR scanners, as compared with several seconds on late-generation CT scanners, make NMR impractical at the present time as an initial screening examination.

The best application of NMR imaging of the spine appears to be in the evaluation of the spinal cord. The contrast between spinal cord and surrounding low-signal-intensity CSF allows easy evaluation of the spinal cord without the need of contrast agents. The usefulness of NMR in the evaluation of syringohydromyelia has been demonstrated [9]. In our five cases, the method yielded completely accurate results. Likewise, a cystic spinal cord tumor was seen very well. Sagittal NMR images provided delineation of the entire extent of the lesion, including the cystic component, to a degree previously possible only with CT metrizamide myelography.

A fatty lesion, with high proton density and short $T_1$ relaxation time, characteristically has a very high signal intensity on NMR images. This was illustrated in three cases of lipoma, two of which occurred in association with spinal

dysraphism. Intra- and extradural lipomas were well delineated, as was the low-lying spinal cord as it merged into the lipoma. In these cases, direct sagittal NMR images were superior to those of other imaging methods.

While our knowledge of characteristic abnormal tissue signals is still elementary, alteration in the expected approximate signal strength from a given tissue can indicate the presence of an abnormality. This is illustrated in the six study cases of vertebral metastases and eosinophilic granuloma, where the architecture of the affected vertebral marrow cavities was probably changed due to decrease of the fat content of the marrow, concomitant with the alteration in both $T_1$ and $T_2$ relaxation times, thus downgrading the signal intensity. Although the diagnosis was readily inferred from other imaging methods, NMR images provided a different parameter on the pathology by demonstrating the involvement of the marrow cavity directly. It is conceivable that this principle will allow NMR to detect early manifestations of pathology that would not be visible with other imaging methods.

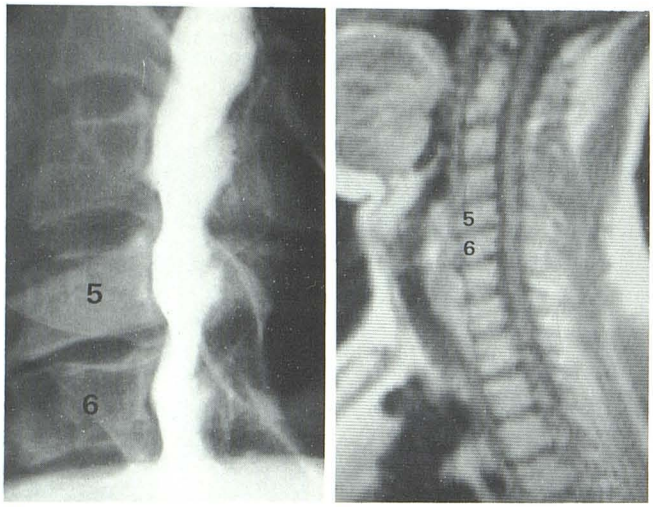


Fig. 15.—Spondylosis with multiple extradural defects. **A**, Pantopaque myelogram. **B**, Sagittal SR image. Osteophytes along posterior aspect of vertebral body at C5–C6 level are seen clearly. Also, there is abnormal buckling of spinal cord at same level.

While herniated disks could not be visualized with NMR, all of the involved disks displayed a lower signal intensity. This was seen in a case of bulging disks without apparent herniation, indicating that the change in signal intensity does not necessarily reflect extrusion of a disk. Rather, it most likely represents change in the chemical composition of the nucleus pulposus, resulting either from degeneration or mechanical causes. At this time, it is not certain whether this finding is of predictive value in the diagnosis of disk herniation.

NMR promises a form of in vivo tissue analysis, and, in the cases outlined above, it nearly succeeded. However, NMR was not as successful in gray-and-white-matter discrimination in the spinal cord as it was in the brain. Our one case of demyelinating disease of the spinal cord showed a questionable, inhomogeneous signal intensity in the area of the thoracic spinal cord, but we find it difficult to interpret these findings because of our limited experience. We must conclude that gray-and-white-matter discrimination below the brainstem is not possible with our present technology. In patients with neurofibromatosis, abnormalities were detected in most of the cases studied, particularly when the signal intensity of the neurofibroma was contrasted against adjacent normal structures. The greatest limitation of NMR in the evaluation of neurofibromatosis as well as intradural meningioma was the plane slice thickness of 10 mm. Partial-volume averaging may lead to false results when the size of the lesion is less than 10 mm. Care must be taken to delineate a small abnormality, particularly when the signal intensity of the abnormal areas is similar to that of surrounding normal structures.

Thinner slices can be obtained on our NMR imager by applying a stronger selection gradient of the magnetic field along the normal direction of the chosen image plane. Magnification is also possible by applying a stronger imaging gradient while the data are being acquired. However, in

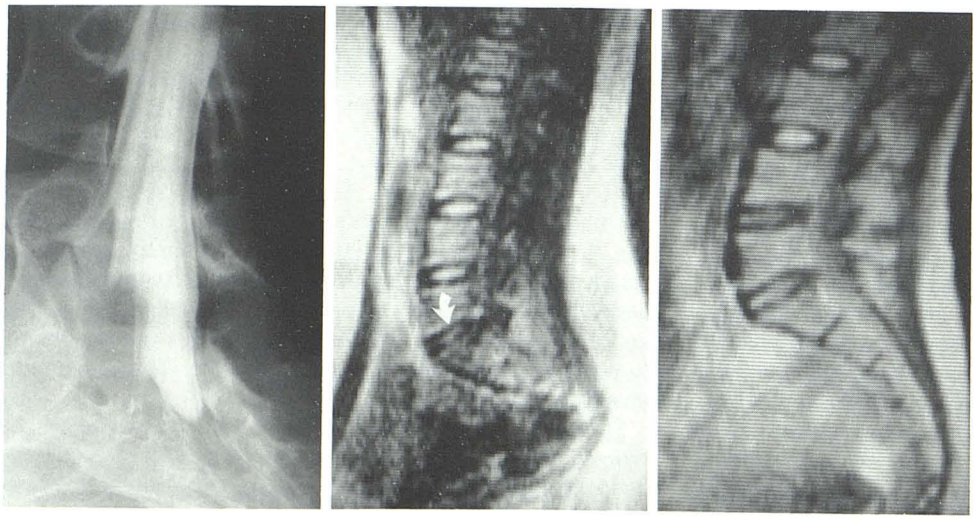


Fig. 16.—Surgically proven herniated disk at L5–S1 in 24-year-old woman. **A**, Metrizamide myelogram shows classical appearance of extradural defect from herniated disk. **B**, $T_2$-weighted SE image shows abnormally low signal intensity of nucleus pulposus at diseased disk level (*arrow*), as compared with normal disk spaces above.

Fig. 17.—Bulging disks in 37-year-old man with low back pain of several months' duration. $T_2$-weighted SE image shows low signal intensity of nucleus pulposus at L4–L5 and L5–S1 levels. Metrizamide myelography on same day did not reveal any evidence of disk herniation, but there was minimal bulging of disks.

both instances, there will be a significant reduction in the signal-to-noise ratio in the images unless this reduction is recovered by signal-averaging, at the expense of markedly prolonged scanning time.

Proper positioning appears to be an essential requirement for good images, particularly in the sagittal plane. The problem is greatly exaggerated in patients with scoliosis. In such cases, examination requires numerous images in different planes and significantly prolongs examination time. These difficulties would be partly solved with three-dimensional imaging, which, unfortunately, was not available to us at the time of our study.

The negative or low signal of compact, cortical bone is a major drawback in the evaluation of the spine, as spinal stenosis and spondylosis cannot be adequately assessed. Because current imaging technique relies on the proton density conspicuously absent in compact bone, bone imaging must await further development in signal generation.

NMR imaging provides a new perspective on abnormalities of the spine; however, greater technical flexibility is needed before the full potential of NMR imaging of the spine can be realized fully.

ACKNOWLEDGMENTS

We thank Mark Clampitt for technical assistance, Joseph Molter for photographic assistance, Bonnie Hami for editing, and Martha Shannon for manuscript preparation.

REFERENCES

1. Alfidi RJ, Haaga JR, El Yousef SJ, et al. Preliminary experimental results in humans and animals with a superconducting, whole-body, nuclear magnetic scanner. *Radiology* **1982**; 143:175–181
2. Bydder GM, Steiner RE, Young IR, et al. Clinical NMR imaging of the brain: 140 cases. *AJNR* **1982**;3:459–480, *AJR* **1982**;139:215–236
3. Brant-Zawadzki M, Davis PL, Crooks LE, et al. NMR demonstration of cerebral abormalities: comparison with CT. *AJNR* **1983**;4:117–124, *AJR* **1983**;140:847–854
4. Young IR, Burl M, Clarke GJ, et al. Magnetic resonance properties of hydrogen: imaging the posterior fossa. *AJNR* **1981**;2:487–493, *AJR* **1981**;137:894–901
5. Kramer DM, Schneider JS, Rudin AM, Lauterbur PC. True three-dimensional nuclear magnetic resonance zeugmatographic images of a human brain. *Neuroradiology* **1981**;21:239–244
6. Hinshaw WS, Andrew ER, Bottomley PA, Holland GN, Moore WS, Worthington BS. Display of cross-sectional anatomy by nuclear magnetic resonance imaging. *Br J Radiol* **1978**;51:273–280
7. Crooks LE, Grover TP, Kaufman L, Singer JR. Tomographic imaging with nuclear magnetic resonance. *Invest Radiol* **1978**;13:63–66
8. Pykett IL, Newhouse JH, Buonanno FS, et al. Principles of nuclear magnetic resonance imaging. *Radiology* **1982**;143:157–168
9. Yeates A, Brant-Zawadzki M, Norman D, Kaufman L, Crooks LE, Newton TH. Nuclear magnetic resonance imaging of syringomyelia. *AJNR* **1983**;4:234–237